INTERNATIONAL JOURNAL FOR NUMERICAL METHODS IN FLUIDS
Int. J. Numer. Meth. Fluids 2007; **53**:1197–1219
Published online 6 July 2006 in Wiley InterScience (www.interscience.wiley.com). DOI: 10.1002/fld.1238

A node-centred finite volume formulation for the solution of two-phase flows in non-homogeneous porous media

D. K. E. de Carvalho[1,*,†], R. B. Willmersdorf[2] and P. R. M. Lyra[2]

[1]*Departamento de Engenharia Civil, UFPE, Av. Acadêmico Hélio Ramos s/n, CEP: 50740-530, Recife—PE, Brazil*
[2]*Departamento de Engenharia Mecânica, UFPE, Av. Acadêmico Hélio Ramos s/n, CEP: 50740-530, Recife—PE, Brazil*

SUMMARY

The simulation of two-phase flow of oil and water in inhomogeneous porous media represents a great challenge because rock properties such as porosity and permeability can change abruptly throughout the reservoir. This fact can produce velocities which vary several orders of magnitude within very short distances. The presence of complex geometrical features such as faults and deviated wells is quite common in reservoir modelling, and unstructured mesh procedures, such as finite elements (FE) and finite volume (FV) methods can offer advantages relative to standard finite differences (FD) due to their ability to deal with complex geometries and the easiness of incorporating mesh adaptation procedures. In fluid flow problems FV formulations are particularly attractive as they are naturally conservative in a local basis. In this paper, we present an unstructured edge-based finite volume formulation which is used to solve the partial differential equations resulting from the modelling of the immiscible displacement of oil by water in inhomogeneous porous media. This FV formulation is similar to the edge-based finite element formulation when linear triangular elements are employed. Flow equations are modelled using a fractional flux approach in a segregated manner through an IMplicit Pressure-Explicit Saturation (IMPES) procedure. The elliptic pressure equation is solved using a two-step approach and the hyperbolic saturation equation is approximated through an artificial diffusion method adapted for use on unstructured meshes. Some representative examples are shown in order to illustrate the potential of the method to solve fluid flows in porous media with highly discontinuous properties. Copyright © 2006 John Wiley & Sons, Ltd.

KEY WORDS: finite volume formulation; two-phase flows; non-homogeneous porous media; edge-based data structure

*Correspondence to: D. K. E. de Carvalho, Departamento de Engenharia Civil, UFPE, Av. Acadêmico Hélio Ramos s/n, CEP: 50740-530, Recife—PE, Brazil.
†E-mail: dkarlo@uol.com.br

Contract/grant sponsor: National Petroleum Agency (ANP)
Contract/grant sponsor: Brazilian Research Council (CNPq)

Received 18 July 2005
Revised 9 March 2006
Accepted 19 March 2006

1. INTRODUCTION

The main objective of the simulation of two-phase flows in porous media is to properly depict the complex physical and chemical fluid flow interactions in order to correctly predict the fluid flow displacement within heterogeneous reservoir rocks. In typical rock formations, porous media heterogeneities range from the pore level to the reservoir scale [1]. Rock properties, such as porosity and permeability may change significantly from one region to another, suffering strong discontinuous variations that generate velocity fields which may vary several orders of magnitude over relatively short distances. Due to this fact, the simulation of fluid flow of oil and water in inhomogeneous porous media generally poses a great challenge for most of the numerical tools available.

One of the most popular methodologies used to describe the fluid flow in petroleum reservoir simulation is the IMplicit Pressure-Explicit Saturation (IMPES) procedure [1–3]. In this technique, a sequential time stepping procedure is used to split the computation of the pressure field from the saturation field. In the IMPES method, initially, the pressure equation is solved implicitly from an initial saturation distribution, and then, velocities are computed from this pressure field. In sequence, the velocity field is used as an input for the saturation equation, which is finally solved explicitly. The process is repeated until the end of the analysis.

The pressure field is governed by a parabolic/elliptic-type equation that can have strong discontinuous coefficients (i.e. permeabilities) and, in general, the saturation equation is similar to a convection–diffusion-type equation, in which the diffusion coefficients are associated to capillary effects. In many situations, capillarity is small and can be neglected. In such cases, the saturation equation behaves essentially as a first-order non-linear hyperbolic conservation law.

Various numerical methods have been devised to solve the partial differential equations associated to the IMPES procedure. The most commonly used are the finite difference (FD) methods which are the standard in petroleum reservoir industry, because they are fast, accurate and simple to implement [1, 2]. Some of the major drawbacks related to FD are their limited ability to properly discretize complex geometries which are common in reservoir modelling, such as, faults, channels and deviated wells, and the difficulty to incorporate automatic mesh adaptive procedures due to the limitations imposed by structured meshes.

Over the last decades, much effort has been put in methods that make use of unstructured meshes, such as the finite element (FE) methods and finite volume (FV) methods due the fact that these methods allow for better modelling of complex geometrical features and because they can easily incorporate mesh adaptive procedures. Finite volume methods are particularly attractive as they conserve mass, globally and locally. Apart from the traditional FD, FE and FV methods, many variations and combinations of numerical methods have been devised for reservoir simulation.

Mass conservative schemes, such as the mixed finite element method (MFEM) and flux continuous finite volumes (FCFV) have been extensively studied in literature [1, 4–8]. In the MFEM, pressure and velocities are approximated simultaneously with the same order of accuracy, and the saturation equation is generally solved using some shock capturing scheme [1, 4]. The recently developed FCFV are defined by assuming continuous pressures and fluxes across control volumes (CV) interfaces [5–8]. Both methods are capable of handling full tensors pressure equations in highly non-homogeneous porous media using structured or unstructured meshes. Another interesting conservative approach involves the so-called control

volume function approximation method (CVFA), in which functions of different types are used to approximate pressure and velocity independently, using arbitrary mesh types [3, 9]. In these references, the saturation equation is solved through an upwind-type method.

Galerkin-type methods have also been designed to solve fluid flows in porous media [10, 11]. One procedure that has been originally developed for the solution of miscible flows in heterogeneous and anisotropic media involves the direct use of the Galerkin FE method to solve the pressure equation, and a velocity post-processing technique to reinforce mass conservation [10]. In this approach, the saturation equation has been solved via a streamline upwind Petrov Galerkin (SUPG) method.

In the last years, combinations of finite elements and finite volumes (FEFVM) have also been used in literature [12, 13]. In these methods, mixed finite elements or Galerkin finite elements with some velocity recovery are used to solve the pressure–velocity problem, and the saturation equation is solved by node-centred [12], or cell-centred [13] conservative finite volumes. In the formulation used in Reference [13], the fluid pressure field is computed using the standard Galerkin FE method with fluid velocities being constant within each finite element. The FV grid is then constructed using a median dual sub-grid, taking advantage of the fact that fluid velocities, which are discontinuous between two elements of the mesh, are continuous through CV faces of the dual grid.

In this work, we present a node-centred conservative fully finite volume formulation in which median dual CV (Donald's dual) are used with an edge-based data structure [14–18] in such a way that the geometrical coefficients are associated to the edges and nodes of the primal mesh. This formulation has been chosen due to the fact that node-centred FV schemes are usually superior to cell-centred schemes in terms of memory usage [14, 15], and because edge-based data structures are known to be more computationally efficient than their element-based counterparts [15].

This FV formulation, which has been recently developed for the solution of two-dimensional two-phase flow problems in an IMPES procedure for homogeneous porous media [16], is further improved to include the capability of simulating two-phase flows in heterogeneous porous media. In our approach, the finite volume method is used to accurately solve both, the elliptic pressure equation and the hyperbolic saturation equation. For the solution of the pressure equation, we devise an alternative way of computing continuous diffusive fluxes through CV faces in heterogeneous media with strong discontinuous coefficients by a modification of Crumpton's two-step approach [17]. The hyperbolic saturation equation is solved using a higher order artificial diffusion scheme which is adapted for use with multidimensional unstructured meshes, and that combines adaptively, second- and fourth-order diffusion terms controlled by a saturation switch [16, 19–21].

2. MATHEMATICAL FORMULATION

In this section, we briefly describe the governing equations for incompressible, immiscible two-phase flows of water and oil through rigid porous media. This model (which can be directly extended to miscible, three-phase flow) is obtained combining Darcy's law with the mass conservation equation for each phase. The formulation adopted here has been successfully used by many authors [1–4, 9, 12, 13, 16], though it is still not commonly used in commercial reservoir simulators.

First, we assume that the phase velocities obey the Darcy's law, which, ignoring gravitational effects can be written for phase i, as

$$\mathbf{v}_i = -\underset{\sim}{\lambda}_i \nabla P_i \tag{1}$$

where the phase mobility tensor is defined as

$$\underset{\sim}{\lambda}_i = \underset{\sim}{K}\frac{k_i}{\mu_i} \quad \text{or} \quad \underset{\sim}{\lambda}_i = \underset{\sim}{K}\lambda_i \tag{2}$$

Here, $\underset{\sim}{K}$ denotes the absolute permeability tensor of the rock, $\lambda_i = k_i/\mu_i$ is the scalar phase mobility, with k_i being the phase relative permeability and μ_i the phase viscosity. Henceforth, we will assume incompressible medium and fluids. We will also ignore the capillary pressure and assume that $P = P_\mathrm{w} = P_\mathrm{o}$, where (w) and (o) stand, respectively, for the wetting (water) and the non-wetting (oil) phases. Additionally, conservation of mass for each phase i can be written as

$$-\nabla \cdot (\rho_i \mathbf{v}_i) + q_i = \frac{\partial(\phi \rho_i S_i)}{\partial t} \tag{3}$$

In (3), ϕ is the porosity, i.e. fraction of the rock which can be occupied by fluids, q_i denotes sources or sinks, ρ_i the phase density and S_i the saturation of phase i, which represents the percentage of the available pore volume occupied by this phase. Due to this last definition, we can write

$$S_\mathrm{o} + S_\mathrm{w} = 1 \tag{4}$$

Combining Equations (1)–(4), and after some algebraic manipulation we obtain the following pressure equation:

$$\nabla \cdot (\underset{\sim}{\lambda} \nabla P) = -Q \quad \text{or} \quad \nabla \cdot \mathbf{v} = Q \tag{5}$$

where $\underset{\sim}{\lambda} = \underset{\sim}{\lambda}_\mathrm{o} + \underset{\sim}{\lambda}_\mathrm{w}$ is the total fluid mobility tensor, $\mathbf{v} = \mathbf{v}_\mathrm{o} + \mathbf{v}_\mathrm{w} = -\underset{\sim}{\lambda} \nabla P$ is the total velocity field and $Q = Q_\mathrm{w} + Q_\mathrm{o}$, with $Q_i = (q_i/\rho_i)$, is the total injection or production specific rate. By introducing the fractional flow function $f_i = \lambda_i/(\lambda_\mathrm{o} + \lambda_\mathrm{w})$, we can also derive a hyperbolic equation for the water saturation, which can be written as

$$\phi \frac{\partial S_\mathrm{w}}{\partial t} + \nabla \cdot \mathbf{F}_\mathrm{w}(S_\mathrm{w}) = Q_\mathrm{w} \tag{6}$$

The term $\mathbf{F}_\mathrm{w} = f_\mathrm{w}\mathbf{v}$ is the flux function which is dependent on the water-phase saturation. As it can be seen, the pressure and saturation fields are connected through the total velocity $\mathbf{v}$.

3. FINITE VOLUME FORMULATION

In the present work, we have adopted a node-centred, median dual CV technique, in which the coefficients necessary to our calculation are associated to the edges and to the nodes of the mesh [14–18]. These edge and node coefficients are pre-computed in a pre-processing

stage from the more traditional element-based data structure which is commonly used in the finite element method [22].

Even though, there is, in principle, no restriction to the shape of the elements utilized to discretize the spatial domain, it is important to keep in mind that edge-based FV schemes are only linearly preserving (i.e. they exactly represent a linear field) on triangular (2D), tetrahedral (3D) or structured quadrilateral (2D) and hexahedral (3D) meshes [23]. Therefore, extra care must be taken when using different element types, especially when considering distorted meshes.

The median dual CV adopted are built connecting centroids of elements to the middle point of the edges that surround a specific mesh node. In edge-based node-centred schemes, fluxes are usually integrated on the dual mesh through one or more loops over the edges, and the computational cost is, essentially, proportional to the number of edges of the mesh. In order to properly handle material discontinuities, we perform the integration over the whole domain in a sub-domain by sub-domain approach, where a sub-domain is defined by a group of elements that share the same physical properties such as permeability and porosity.

Node-centred finite volume schemes in which physical properties are uniform in the elements of the primal mesh are named 'cell distributed schemes' in opposition to the so-called 'point distributed schemes' in which properties are uniform inside the CV of the dual mesh [7, 8, 24].

In this work, we have chosen to use the cell distributed methodology due to the easiness of associating rock properties to sub-domains which encompass groups of elements (e.g. triangles or tetrahedral) that naturally fit to reservoir bed boundaries.

In what follows, we will show how to derive an edge-based FV method which is naturally capable of handling heterogeneous materials.

3.1. Implicit pressure equation

In order to obtain our discrete equations, we can write

$$\nabla \cdot \mathbf{v} = Q \tag{7}$$

Integrating (7) over the domain and using the Gauss–Green theorem, yields

$$\int_{\Gamma} \mathbf{v} \cdot \mathbf{n} \partial\Gamma = \int_{\Omega} Q \partial\Omega \tag{8}$$

Finally, for a node I of the mesh, we can write the discrete form of (8), as

$$\sum_{L_{I(\Omega)}} \mathbf{v}^{\Omega}_{IJ_L} \cdot \mathbf{C}_{IJ_L} + \sum_{L_{I(\Gamma)}} \mathbf{v}^{\Gamma}_{IJ_L} \cdot \mathbf{D}_{IJ_L} = Q_I V_I \tag{9}$$

In (9), V_I is the volume of the CV surrounding node I, the upper index Ω represents approximations on the middle of every edge IJ_L of the mesh which is connected to node I and Γ refers only to boundary edges connected to that node and the summation is performed over the edges (L_I) connected to node I. The geometrical coefficients $\mathbf{C}_{IJ_L}$ and $\mathbf{D}_{IJ_L}$ are defined as

$$\begin{aligned} \mathbf{C}_{IJ_L} &= A_{K+1}\mathbf{n}_{K+1} + A_K \mathbf{n}_K \\ \mathbf{D}_{IJ_L} &= A_L \mathbf{n}_L \end{aligned} \tag{10}$$

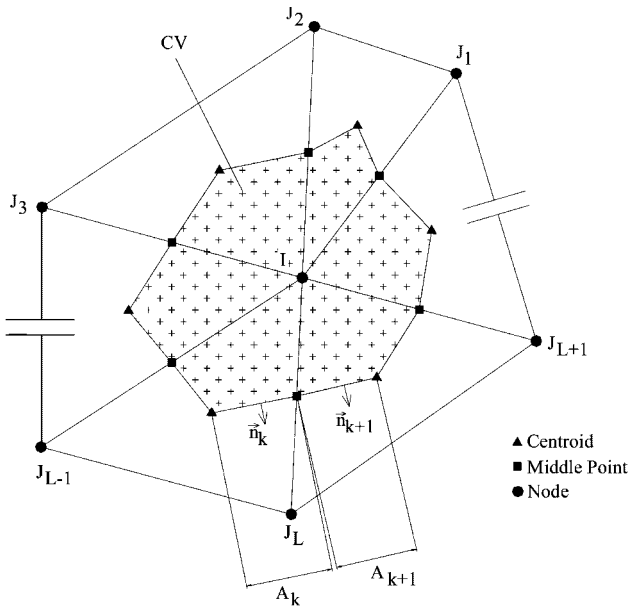

Figure 1. 2-D internal CV.

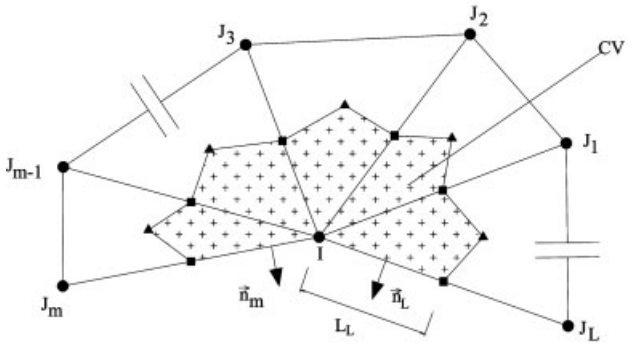

Figure 2. 2-D boundary CV.

In (10), $A_K = TL_K$, $A_{K+1} = TL_{K+1}$ and $A_L = TL_L$ are the areas of the CV faces associated to the normals $\mathbf{n}_K$, $\mathbf{n}_{K+1}$ and $\mathbf{n}_L$, respectively, and T is the thickness of the domain. Figures 1 and 2 show some details of the internal and boundary CV and their geometrical parameters for a typical triangular mesh. Further details can be found in References [16, 25].

In order to approximate the mid-edge gradients/velocities required in (9), different strategies can be devised [26]. A classical approach involves using a simple two-point approximation in which mid-edge velocities are formally second-order accurate only if the media is isotropic and the straight lines that connects two adjacent nodes and the CV faces are orthogonal to

each other as in the case of the Voronoi tessellations [6, 7]. Schemes using such approaches are equivalent to the so-called control volume finite difference methods (CVFD).

In the present paper, we use a different approach which has been originally devised by Crumpton *et al*. [17] for the discretization of diffusion terms in the Navier–Stokes equations. In this approach, in order to obtain the final discrete system of equations, we first determine nodal gradients as functions of the discrete pressure field and then, we use these gradients to compute the elliptic terms in a second step [14, 16–18, 25, 27].

Again, we make use of the Gauss–Green theorem to integrate the pressure gradient at node I, obtaining

$$\int_{\Omega_I} \nabla P_I \partial\Omega_I = \int_{\Gamma_I} P_I \mathbf{n} \partial\Gamma \tag{11}$$

Assuming that the average gradient in the CV can be defined as

$$\bar{\nabla} P_I V_I = \int_{\Omega_I} \nabla P_I \partial\Omega_I \tag{12}$$

we can write the discrete form of (11) as

$$\nabla P_I V_I = \left(\sum_{L_{I(\Omega)}} P^{\Omega}_{IJ_L} \mathbf{C}_{IJ_L} + \sum_{L_{I(\Gamma)}} P^{\Gamma}_{IJ_L} \mathbf{D}_{IJ_L} \right) \tag{13}$$

Further, we must adopt the following linear edge approximations:

$$P^{\Omega}_{IJ_L} = \frac{P_I + P_{J_L}}{2} \quad \text{and} \quad P^{\Gamma}_{IJ_L} = \frac{5P_I + P_{J_L}}{6} \tag{14}$$

Inserting (14) in (13), we obtain

$$\nabla P_I = \frac{1}{V_I} \left[\sum_{L_{I(\Omega)}} \mathbf{C}_{IJ_L} \frac{(P_I + P_{J_L})}{2} + \sum_{L_{I(\Gamma)}} \mathbf{D}_{IJ_L} \frac{(5P_I + P_{J_L})}{6} \right] \tag{15}$$

The boundary term ($P^{\Gamma}_{IJ_L}$) defined in (14) assumes a piecewise linear interpolation for boundary fluxes similar to a FE-type approximation, being formally second-order accurate in space when linear triangles are used [15]. A simpler methodology which is commonly used in FV formulations is to consider a piecewise constant approximation for the boundary flux term, i.e. $P^{\Gamma}_{IJ_L} = P_I$. This last approach, which is independent of the type of the elements used for the spatial discretization, can be used with some loss of accuracy along the boundary faces [14–16].

3.1.1. Heterogeneous porous media. For the heterogeneous media case, fluxes definition over the edges located at the interface between different types of rocks can be ambiguous [11]. If gradients computed as described in (15) are directly used for flux computations, an inconsistent flux would be obtained along CV faces adjacent to rock discontinuities. In order to circumvent this problem, we recover gradients in a sub-domain by sub-domain approach. First we assume that rock properties, such as porosity and permeability are associated to sub-domains. For each physical sub-domain, we store a list of edges and nodes and their associated geometrical coefficients. Considering the mesh shown in Figure 3, it is necessary

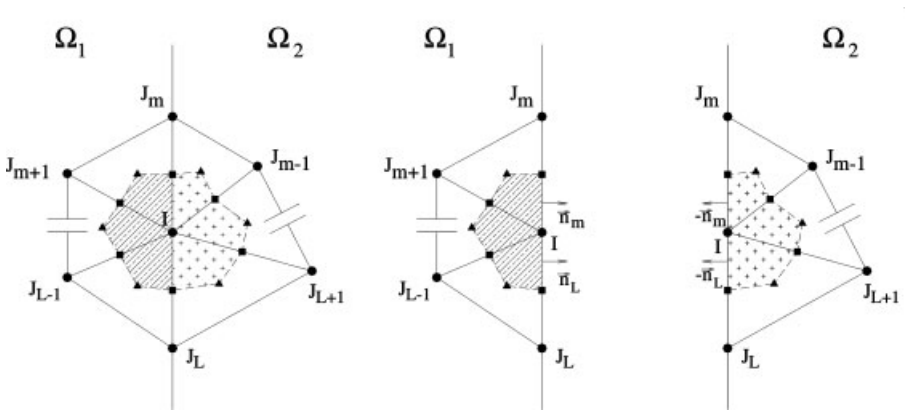

Figure 3. 2-D CV split by two different rock types.

to include new geometrical coefficients $\mathbf{D}_{IJ_L} = A_L \mathbf{n}_L$ and $\mathbf{D}_{IJ_M} = A_M \mathbf{n}_M$, which are related to internal boundary edges, in order to correct reconstruct gradients and fluxes in a particular sub-domain. These coefficients allow for a second-order recovery of gradients for each physical sub-domain of the problem, allowing for a discontinuous flux computation. Therefore, for heterogeneous porous media, we can rewrite (15) as

$$\nabla P_I^{\Omega_R} = \frac{1}{V_I^{\Omega_R}} \left[\sum_{L_{I(\Omega_R)}} \mathbf{C}_{IJ_L}^{\Omega_R} \frac{(P_I + P_{J_L})}{2} + \sum_{L_{I(\Gamma_{RE})}} \mathbf{D}_{IJ_L}^{\Omega_R} \frac{(5P_I + P_{J_L})}{6} + \sum_{L_{I(\Gamma_{RI})}} \mathbf{D}_{IJ_L}^{\Omega_R} \frac{(5P_I + P_{J_L})}{6} \right] \tag{16}$$

In (16), $\nabla P_I^{\Omega_R}$ is the nodal gradient and $V_I^{\Omega_R}$ is the CV of a node I associated to the sub-domain Ω_R, and $\mathbf{C}_{IJ_L}^{\Omega_R}$ and $\mathbf{D}_{IJ_L}^{\Omega_R}$ refer to the geometrical coefficients of the edge IJ_L associated to the same sub-domain Ω_R. Finally, note that in this sub-domain approach, $\mathbf{D}_{IJ_L}^{\Omega_R}$ refers to both, external and internal boundary edges, and Γ_{RE} and Γ_{RI} refer, respectively, to loops over external boundary edges and edges between multiple domains.

After the computation of nodal gradients, a common choice in edge-based schemes involves repeating the same simple strategy used to compute mid-edge-pressures P_{IJ_L} (i.e. the arithmetic mean) of (13) in order to compute mid-edge gradients, producing a two-layer stencil for the approximation of the elliptic terms [14, 26]. However appealing this strategy may look, it must be strongly avoided as it can be proved that, for orthogonal equally spaced meshes (e.g. uniform structured quadrilateral or hexahedral ones), it implies that the values computed at a given node are uncoupled from the values of those nodes directly connected to it, leading to leap-frog modes commonly known as 'checker-boarding' or 'odd–even' oscillations, [14, 16, 25, 26]. Even if non-uniform unstructured triangular or tetrahedral meshes are used in this approach, the simple adoption of this extended stencil and the weak coupling with the directly connected nodes leads to some loss of accuracy and reduction of convergence rates of the resulting scheme [14]. In fact, Svärd and Nordström [26], have proved that this scheme is an inconsistent approximation for the Laplacian (diffusive) operator on general triangular meshes.

In order to overcome such weaknesses, mid-edge gradients and correspondingly velocities must be computed in a different manner. A much better approach, which was originally proposed by Crumpton *et al.* [17], introduces a local compact stencil for the gradient computation along the edge direction, avoiding the odd–even decoupling and recovering second-order accuracy for that part of the gradient [14]. This strategy, which has been recently used for the solution of fluid flows in homogeneous porous media [14, 16], involves a local frame of reference, in which one axis is placed along the edge direction (P), and another axis (N) is orthogonal to the direction (P) as stated in (17)

$$\nabla P_{IJ_L}^{\Omega_R} = \nabla P_{IJ_L}^{\Omega_R(N)} + \nabla P_{IJ_L}^{\Omega_R(P)} \tag{17}$$

The component of the gradient parallel to the edge direction $\nabla P_{IJ_L}^{\Omega_R(P)}$ is replaced by a local second-order central difference approximation $\nabla P_{IJ_L}^{\Omega_R(P^*)}$, as follows:

$$\nabla P_{IJ_L}^{\Omega_R^*} = \nabla P_{IJ_L}^{\Omega_R(N)} + \nabla P_{IJ_L}^{\Omega_R(P^*)} \tag{18}$$

where

$$\nabla P_{IJ_L}^{\Omega_R(P^*)} = \frac{(P_{J_L} - P_I)}{|\Delta_{IJ_L}|}\mathbf{L}_{IJ_L} \tag{19}$$

In (19), $|\Delta_{IJ_L}|$ and $\mathbf{L}_{IJ_L} = \overline{IJ_L}/|\Delta_{IJ_L}|$ are, respectively, the length and the unity vector of the edge IJ_L.

From (17), the normal component of the gradient associated to the edge can be computed as

$$\nabla P_{IJ_L}^{\Omega_R(N)} = \nabla P_{IJ_L}^{\Omega_R} - \nabla P_{IJ_L}^{\Omega_R(P)} \tag{20}$$

where the gradient along the edge direction is given by

$$\nabla P_{IJ_L}^{\Omega_R(P)} = (\nabla P_{IJ_L}^{\Omega_R} \cdot \mathbf{L}_{IJ_L})\mathbf{L}_{IJ_L} \tag{21}$$

with

$$\nabla P_{IJ_L}^{\Omega_R} = \frac{\nabla P_I^{\Omega_R} + \nabla P_{J_L}^{\Omega_R}}{2} \tag{22}$$

Inserting (21) in (20) yields

$$\nabla P_{IJ_L}^{\Omega_R(N)} = \nabla P_{IJ_L}^{\Omega_R} - (\nabla P_{IJ_L}^{\Omega_R} \cdot \mathbf{L}_{IJ_L})\mathbf{L}_{IJ_L} \tag{23}$$

Inserting (19) and (23) in (18), we have

$$\nabla P_{IJ_L}^{\Omega_R^*} = \nabla P_{IJ_L}^{\Omega_R} - (\nabla P_{IJ_L}^{\Omega_R} \cdot \mathbf{L}_{IJ_L})\mathbf{L}_{IJ_L} + \frac{(P_{J_L} - P_I)}{|\Delta_{IJ_L}|}\mathbf{L}_{IJ_L} \tag{24}$$

Defining the continuous 'hybrid' mid-edge velocity as

$$\mathbf{v}_{IJ_L}^{\Omega_R^*} = -\underset{\sim}{\lambda}_{IJ_L}^{\Omega_R} \nabla P_{IJ_L}^{\Omega_R^*} \tag{25}$$

in which, the term hybrid was used to indicate that one part of the mid-edge gradient/velocity (i.e. the cross-diffusion term) is computed using the traditional edge-based finite volume

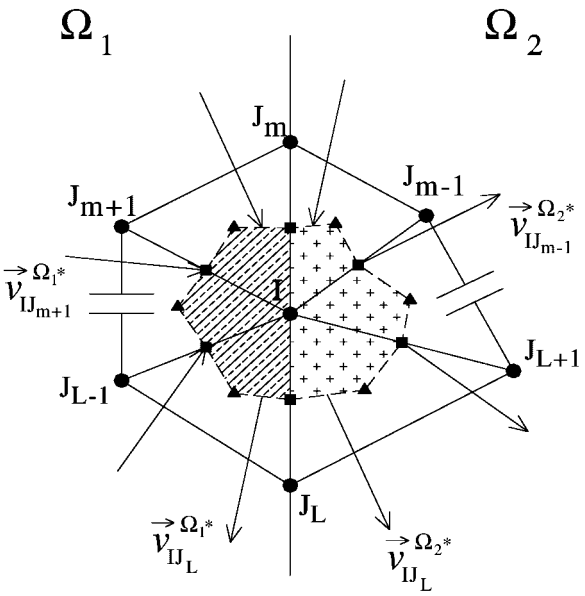

Figure 4. Mid-edge velocities computed for a CV on the interface between two different rock types: $\mathbf{v}_{IJ_L}^{\Omega_1^*}$ the velocity associated to edge IJ_L within rock type Ω_1; $\mathbf{v}_{IJ_L}^{\Omega_2^*}$ the velocity associated to edge IJ_L within rock type Ω_2.

approach by averaging the nodal Green–Gauss gradients, and the other part is computed using the compact two point finite difference scheme.

Inserting (24) in (25), we can write

$$\mathbf{v}_{IJ_L}^{\Omega_R^*} = -\underset{\sim}{\lambda}_{IJ_L}^{\Omega_R}\left(\nabla P_{IJ_L}^{\Omega_R} - (\nabla P_{IJ_L}^{\Omega_R}\cdot\mathbf{L}_{IJ_L})\mathbf{L}_{IJ_L} + \frac{(P_{J_L}-P_I)}{|\Delta_{IJ_L}|}\mathbf{L}_{IJ_L}\right) \tag{26}$$

Using (22) in (26), we can also write the hybrid mid-edge velocity, as

$$\mathbf{v}_{IJ_L}^{\Omega_R^*} = -\underset{\sim}{\lambda}_{IJ_L}^{\Omega_R}\left(\frac{(\nabla P_I^{\Omega_R}+\nabla P_{J_L}^{\Omega_R})}{2} - \left(\frac{(\nabla P_I^{\Omega_R}+\nabla P_{J_L}^{\Omega_R})}{2}\cdot\mathbf{L}_{IJ_L}\right)\mathbf{L}_{IJ_L} + \frac{(P_{J_L}-P_I)}{|\Delta_{IJ_L}|}\mathbf{L}_{IJ_L}\right) \tag{27}$$

In this work, we have dealt only with isotropic porous media, therefore we have assumed that $\underset{\sim}{\lambda}_{IJ_L}^{\Omega_R} = \underset{\sim}{K}^{\Omega_R}\lambda_{IJ_L}$, where $\underset{\sim}{K}^{\Omega_R} = k^{\Omega_R}\underset{\sim}{I}$, with k^{Ω_R} being constant for each sub-domain Ω_R, and $\underset{\sim}{I}$ is the identity matrix. The edge values of the scalar mobility terms are approximated using a mid-point rule in order to formally guarantee second-order accuracy [14, 28], i.e. $\lambda_{IJ_L} = (\lambda_I + \lambda_{J_L})/2$ and viscosity is constant under the assumption of incompressible flow.

Figure 4 shows schematically the mid-edge velocities computed for a CV encompassing two different materials. Note that for interface edges (e.g. IJ_L) two independent velocities are separately computed.

Now, we can redefine (9) using this new mid-edge velocity approximation as

$$\sum_{R=1}^{\text{Ndom}} \left(\sum_{L_{I(\Omega_R)}} \mathbf{v}_{IJ_L}^{\Omega_R^*} \cdot \mathbf{C}_{IJ_L}^{\Omega_R} + \sum_{L_{I(\Gamma_R)}} \mathbf{v}_{IJ_L}^{\Gamma} \cdot \mathbf{D}_{IJ_L}^{\Omega_R} \right) = Q_I V_I \tag{28}$$

and Ndom refers to the number of domains that surrounds node I.

Finally, inserting (27) in (28), the discrete pressure equation for a node I, considering the contributions of a sub-domain Ω_R can be written as

$$\sum_{R=1}^{\text{Ndom}} \left[\sum_{L_I(\Omega_R)} \left(-\underset{\sim}{\lambda}_{IJ_L}^{\Omega_R} \left(\frac{(\nabla P_I^{\Omega_R} + \nabla P_{J_L}^{\Omega_R})}{2} - \left(\frac{(\nabla P_I^{\Omega_R} + \nabla P_{J_L}^{\Omega_R})}{2} \cdot \mathbf{L}_{IJ_L} \right) \mathbf{L}_{IJ_L} + \frac{(P_{J_L} - P_I)}{|\Delta_{IJ_L}|} \mathbf{L}_{IJ_L} \right) \right) \cdot \mathbf{C}_{IJ_L}^{\Omega_R} \right]$$

$$= Q_I V_I - \sum_{R=1}^{\text{Ndom}} \left(\sum_{L_I(\Gamma_R)} \mathbf{v}_{IJ_L}^{\Gamma} \cdot \mathbf{D}_{IJ_L}^{\Omega_R} \right) \tag{29}$$

The nodal values $\nabla P_I^{\Omega_R}$ and $\nabla P_{J_L}^{\Omega_R}$ are computed using the expression given by (16). Further, it is worthy mentioning that the boundary terms in (29) are different from zero only in the case of non-homogeneous Neumann boundary conditions.

It must be emphasized that the expression above is built in a sub-domain by sub-domain basis (i.e. looping over sub-domains) in order to formally guarantee that nodal gradients and velocities are correctly approximated for each material (i.e. rock type) along interface edges. When (29) is written for all mesh nodes, this approach produces, in general, a non-symmetric system of equations that is assembled in a sub-domain approach which been solved using a simple sparse Gauss elimination solver.

3.2. The explicit saturation equation

It is well known that space-centred discretizations, such as Galerkin FE and centred FD, produce unstable numerical schemes when used to discretize advective terms that characterize hyperbolic conservation laws (e.g. saturation equation). Besides, the concept of numerical artificial diffusion plays an essential role in attempting to stabilize and to eliminate spurious oscillations close to discontinuities when these central difference-type methods are used [21].

The formulation we have used in the present work was originally proposed by Jameson *et al.* [19], with the modifications presented in References [20, 21]. This method is based on the utilization of an adaptive 'artificial viscosity' term that combines both, second- and fourth-order dissipative terms. The basic idea of the method is to use the second-order values in regions of high gradients and to introduce the fourth-order terms only in regions of smooth gradients in order to stabilize the scheme.

By integrating (6), we can write

$$\int_\Omega \phi \frac{\partial S_\mathrm{w}}{\partial t} \partial\Omega + \int_\Omega \nabla \cdot \mathbf{F}_\mathrm{w}(S_\mathrm{w}) \partial\Omega = \int_\Omega Q_\mathrm{w} \partial\Omega \tag{30}$$

Using the Green–Gauss theorem, we obtain

$$\int_\Omega \phi \frac{\partial S_\mathrm{w}}{\partial t} \partial\Omega + \int_\Gamma \mathbf{F}_\mathrm{w}(S_\mathrm{w}) \cdot \mathbf{n} \partial\Gamma = \int_\Omega Q_\mathrm{w} \partial\Omega \tag{31}$$

Considering the general case of an inhomogeneous porous media, a semi-discrete numerical scheme for the solution of the non-linear hyperbolic saturation equation, can be written as

$$\frac{\partial S_{\mathrm{w}}}{\partial t} = -\frac{1}{(\phi V)_I^{\mathrm{avg}}} \left(\sum_{R=1}^{\mathrm{Ndom}} \left(\sum_{L_I(\Omega_R)} \mathbf{F}_{IJ_L(\mathrm{w})}^{\Omega_R} \cdot \mathbf{C}_{IJ_L}^{\Omega_R} + \sum_{L_I(\Gamma)} \mathbf{F}_{IJ_L(\mathrm{w})}^{\Gamma_R} \cdot \mathbf{D}_{IJ_L}^{\Omega_R} \right) - Q_{\mathrm{w}} V_I \right) \tag{32}$$

Where the volume-averaged porosity for a node I is defined as

$$(\phi V)_I^{\mathrm{avg}} = \sum_{R=1}^{\mathrm{Ndom}} \phi^{\Omega_R} V_I^{\Omega_R} \tag{33}$$

in which ϕ^{Ω_R} refers to the porosity of sub-domain Ω_R, and $V_I^{\Omega_R}$ is the volume of sub-domain Ω_R associated to node I.

For a node which do not belong to an interface between multiple sub-domains the volume-averaged porosity is simply

$$(\phi V)_I^{\mathrm{avg}} = \phi^{\Omega_R} V_I^{\Omega_R} \tag{34}$$

The boundary flux computed in (32) is null in general to honour the no-flux condition at reservoir boundaries, and the sub-domain mid-edge flux term $\mathbf{F}_{IJ_L(\mathrm{w})}^{\Omega_R} \cdot \mathbf{C}_{IJ_L}^{\Gamma_R}$ is replaced by

$$\mathbf{F}_{IJ_L(\mathrm{w})}^{\Omega_R} \cdot \mathbf{C}_{IJ_L}^{\Omega_R} = \tfrac{1}{2}(\mathbf{F}_{I(\mathrm{w})} + \mathbf{F}_{J_L(\mathrm{w})}) \cdot \mathbf{C}_{IJ_L}^{\Omega_R} + \mathrm{AD} \tag{35}$$

where AD stands for the 'artificial dissipation' term, which can be computed as

$$\mathrm{AD} = -\frac{\alpha_{IJ_L}^{\Omega_R} |\mathbf{C}_{IJ_L}^{\Omega_R}|}{2} [\xi_{IJ_L}^{(2)} \Delta S_{IJ_L} + \xi_{IJ_L}^{(4)} (\Delta S_{IJ_L} - (|\Delta_{IJ_L}| \nabla S_{IJ_L} \cdot \mathbf{L}_{IJ_L}))] \tag{36}$$

The flux function $\mathbf{F}_{IJ_L(\mathrm{w})}^{\Omega_R}$ over the edge is computed as

$$\mathbf{F}_{IJ_L(\mathrm{w})}^{\Omega_R} = \frac{(f_I + f_{J_L})}{2} \mathbf{v}_{IJ_L}^{\Omega_R^*} \tag{37}$$

with $f_{I(\mathrm{w})} = \lambda_{I(\mathrm{w})}/(\lambda_{I(\mathrm{o})} + \lambda_{I(\mathrm{w})})$, and the hybrid mid-edge velocity is consistently obtained by (27).

The gradient of the saturation on the middle of the edge (∇S_{IJ_L}) is computed through a simple arithmetic average as

$$\nabla S_{IJ_L} = \frac{\nabla S_I + \nabla S_{J_L}}{2} \tag{38}$$

and $\Delta S_{IJ_L} = S_{J_L} - S_I$. The nodal gradients ∇S_I and ∇S_{J_L} are obtained using a Green–Gauss reconstruction as described in (15) even for the heterogeneous medium, because in this case, nodal gradients are not used for fluxes computations associated to material properties. Parameters $\xi_{IJ_L}^{(2)}$ and $\xi_{IJ_L}^{(4)}$ are adapted to the fluid flow condition and are defined according to

$$\begin{aligned} \xi_{IJ_L}^{(2)} &= \mu^{(2)} \max(\Upsilon_I, \Upsilon_{J_L}) \\ \xi_{IJ_L}^{(4)} &= \max(0, \mu^{(4)} - \xi_{IJ_L}^{(2)}) \end{aligned} \tag{39}$$

with

$$\Upsilon_I = \frac{|S_{J_L} - 2S_I + S_{I_L}|}{(1-\theta)(|S_{J_L} - S_I| + |S_I - S_{I_L}|) + \theta(S_{J_L} + 2S_I + S_{I_L}) + \varepsilon} \tag{40}$$

In (39) and (40), $\mu^{(2)}$ and $\mu^{(4)}$ and the weighting coefficient θ ($0 \leqslant \theta \leqslant 1$) are user-specified coefficients, and ε is a small constant used only to avoid the appearance of zero in the denominator. In the present paper, we have adopted $\mu^{(2)} = 1.1$, $\mu^{(4)} = 0.85$, $\theta = 0$ and $\varepsilon = 10^{-6}$. The factor Υ_I is a sensor designed to detect discontinuities. For the scaling parameter α_{IJ_L}, we have used the following product: $|\mathbf{v}_{IJ_L}^{\Omega_R^*}||\Delta f_{IJ_L}/\Delta S_{IJ_L}|$ with $\Delta f_{IJ_L}/\Delta S_{IJ_L} = (f_{J_L} - f_I)/(S_{J_L} - S_I)$, when $S_{J_L} \neq S_I$, and $\Delta f_{IJ_L}/\Delta S_{IJ_L} = 0.0$ otherwise, even though other choices could be used [21]. Finally, S_{I_L} is the value of the saturation, obtained through a gradient reconstruction along the edge IJ_L, on a ghost node I_L distant $|\Delta_{IJ_L}|$ to the left from node I. For further details see References [20, 21]. Equation (40) was built in such a way that Υ_I is significant only in regions of strong gradients in order to reduce local oscillations. To preserve the second order of accuracy of the scheme in smooth regions of the flow, and to control the amount of artificial diffusion to be added, the fourth-order dissipation term is turned off (i.e. $\xi_{IJ_L}^{(4)} \equiv 0$) in the presence of strong gradients, while the second-order difference factor $\xi_{IJ_L}^{(2)}$ is activated. This is an important feature because only the second-order term is desired near the flow discontinuity and the fourth-order term must be avoided as it may produce undesirable oscillations.

It is worthy noting that, again, fluxes calculations must be done in a sub-domain by sub-domain basis as described previously for the implicit pressure equation.

After the fluxes are properly calculated, time integration is performed through a simple two-level explicit time step scheme (Euler forward), i.e.

$$S_{\mathrm{w}}^{n+1} = S_{\mathrm{w}}^{n} - \frac{\Delta t}{(\phi V)_I^{\mathrm{avg}}} \left(\sum_{R=1}^{\mathrm{Ndom}} \left(\sum_{L_{I(\Omega)}} \mathbf{F}_{IJ_L(\mathrm{w})}^{\Omega_R} \cdot \mathbf{C}_{IJ_L}^{\Omega_R} \right) - Q_{\mathrm{w}} V_I \right) \tag{41}$$

with $\mathbf{F}_{IJ_L(\mathrm{w})}^{\Omega_R}$ being computed by (35)–(40).

Even though second-order time accuracy is, in general, less important than second-order spatial accuracy as pointed by Durlofsky [13], higher order accurate time integration of the saturation equation can be simply achieved by using a predictor–corrector method or the Runge–Kutta procedure [21].

4. EXAMPLES

4.1. Solution of the elliptic pressure equation in non-homogeneous domains

The problems analysed in this example were adapted from Reference [28] in order to show that the edge-based scheme presented here is capable of handling discontinuous materials even for very coarse meshes. Here, we will consider the solution of the simplest elliptic equation $\nabla(\underset{\sim}{K}\nabla P) = 0$, where $\underset{\sim}{K} = k\,\underset{\sim}{I}$ and k is a scalar discontinuous coefficient.

In Reference [28], the authors adopted a different method for handling heterogeneities, in which permeabilities are directly associated to the edges of the meshes in two steps. First, they are associated to nodes using a volume average procedure, and then, their values

are simply assigned to edges through the arithmetic mean of the correspondent edge node values. Even though, we consider it a valid approximation procedure, we believe our method of evaluating fluxes for CV lying over material discontinuities has a more solid physical background, as the fluxes/velocities at the CV faces, which are used for volumetric balance, are exactly computed in the case of a linear variation of the pressure field.

(a) Initially, we consider a 1×1 square domain, which is split horizontally in two equally spaced parts as shown in Figure 5. The non-dimensional diffusive parameters (i.e. permeabilities) are $\underset{\sim}{K}_{\mathrm{A}} = 10.0\underset{\sim}{I}$ for sub-domain A, and $\underset{\sim}{K}_{\mathrm{B}} = 50.0\underset{\sim}{I}$ for sub-domain B. Boundary conditions are $P_{\mathrm{B}} = 1.0$ on the bottom of the domain and $P_{\mathrm{T}} = 0.0$ on the top of the domain. Homogeneous Neumann boundary conditions are set on the left- and right-hand sides of the domain. Figure 6 shows the extremely coarse triangular mesh adopted and the contours for the scalar variable P. The exact solution for the pressure at $y = 0.5$ is $P = 1/6$, while exact calculated velocities for sub-domains A and B are $v = -k(\partial P/\partial y)_{\mathrm{analytic}} = 100/6$ [28]. The maximum relative errors $E_{\mathrm{rel}} = \max|u^{\mathrm{exat}} - u^{\mathrm{aprox}}|/|u^{\mathrm{exat}}|$, with $u = P$ and $u = v$, are equal to $E_{\mathrm{rel}}^{\mathrm{pressure}} \cong 83.501\%$ for interface nodes and $E_{\mathrm{rel}}^{\mathrm{velocity}} \cong 51.041\%$ for velocities computed at the CV faces using the procedure described in Reference [28].

On the other hand, in our procedure, numerical solutions for both, P and v (e.g. pressures and velocities) computed at the CV faces, are exact to machine precision.

(b) In the second problem, the domain is partitioned vertically in two, as shown in Figure 7. Boundary conditions and the permeabilities are the same of the previous example, i.e. $P_{\mathrm{B}} = 1.0$, $P_{\mathrm{T}} = 0.0$, $\underset{\sim}{K}_{\mathrm{A}} = 10.0\underset{\sim}{I}$ and $\underset{\sim}{K}_{\mathrm{B}} = 50.0\underset{\sim}{I}$. In this case, the analytical solution for nodal pressures at $y = 0.5$, is $P = 0.5$. The exact velocities for sub-domains A and B are $v_{\mathrm{A}} = -k(\partial P/\partial y)_{\mathrm{analytic}} = 10.0$ and $v_{\mathrm{B}} = -k(\partial P/\partial y)_{\mathrm{analytic}} = 50.0$, respectively [28]. In this case, the relative errors for the nodal pressure field and velocities at the CV faces computed using the procedure given in Reference [28] are, respectively, $E_{\mathrm{rel}}^{\mathrm{pressure}} \cong 7.838\%$ and $E_{\mathrm{rel}}^{\mathrm{velocity}} \cong 3.839\%$. Again, in our procedure, numerical solutions for pressures and velocities are obtained exactly. Figure 8 shows the triangular mesh adopted and the contours for the pressure P.

In the two cases shown above, it is clear that our procedure to calculate fluxes/velocities for discontinuous materials is far superior to the volume average procedure proposed in Reference [28], which has produced very poor results for the coarse meshes considered here.

4.2. *Confined flow between two perpendicular barriers*

In this problem, water is injected in the left-hand side of the domain in order to sweep the resident oil. The geometry was obtained from Garcia [29]. The fluid flow occurs due to the difference of pressure in the confined region that has two perpendicular barriers with extremely low permeability zones. Fluid properties are: $\rho_{\mathrm{w}} = \rho_{\mathrm{o}} = 1000\ \mathrm{kg/m^3}$, $\mu_{\mathrm{w}} = 0.001\ \mathrm{kg/m\,s}$ and $\mu_{\mathrm{o}} = 0.004\ \mathrm{kg/m\,s}$. Permeability inside the barriers is $\underset{\sim}{K} = 10^{-10}$ and $10^{-4}\underset{\sim}{I}\ \mathrm{m^2}$ in the rest of the domain, in such a way that permeability varies six orders of magnitude from the barriers to the rest of the reservoir and therefore, these barriers form a channel in which fluid must preferentially flow.

Porosity is $\phi = 0.2$ in the barriers and $\phi = 0.35$ in the rest of the domain. In this example, we have used a quadratic relative permeability relationship [30]. The water and the oil residual

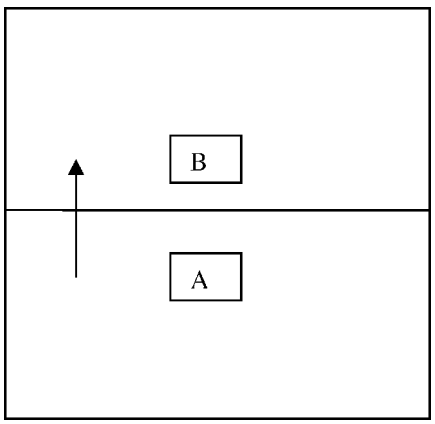

Figure 5. Square horizontally split domain made of two different materials.

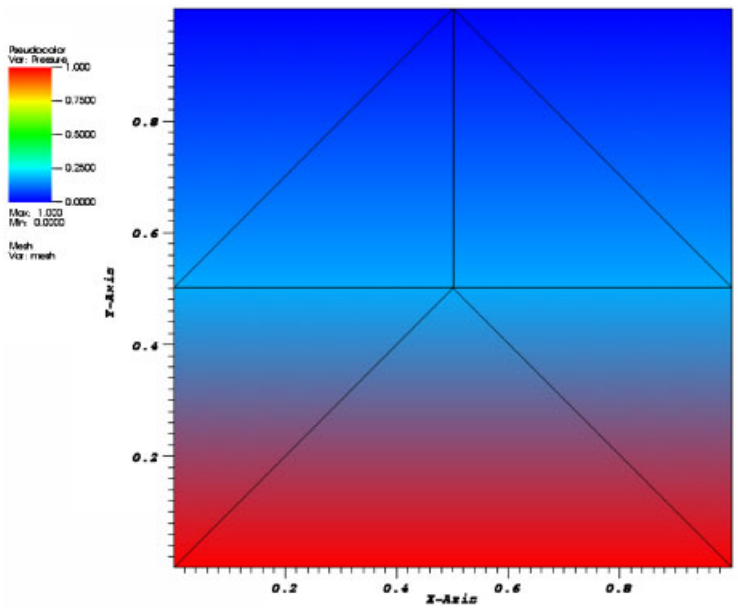

Figure 6. Square horizontally split domain made of two different materials: triangular mesh used to discretize the domain and the contours for the scalar variable P.

saturations are $S_{\mathrm{wr}} = S_{\mathrm{or}} = 0.1$. Boundary conditions for the pressure and for the saturation equations are $P_L = 5.10^3$ Pa and $S_{\mathrm{w}L} = 0.9$ on the left side and $P_R = 1.10^3$ Pa on the right-hand side of the domain. A coarse mesh with 156 nodes, 266 elements and 421 edges was used. Figure 9 shows the geometric configuration of this problem. Figures 10 and 11 show the mesh and the pressure surface contour (i.e. pressure field 'extruded' along Z-axis) for instant

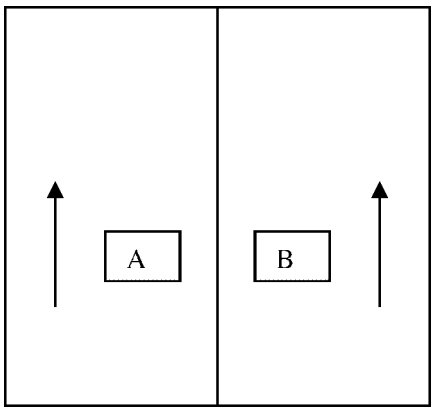

Figure 7. Square vertically split domain made of two different materials.

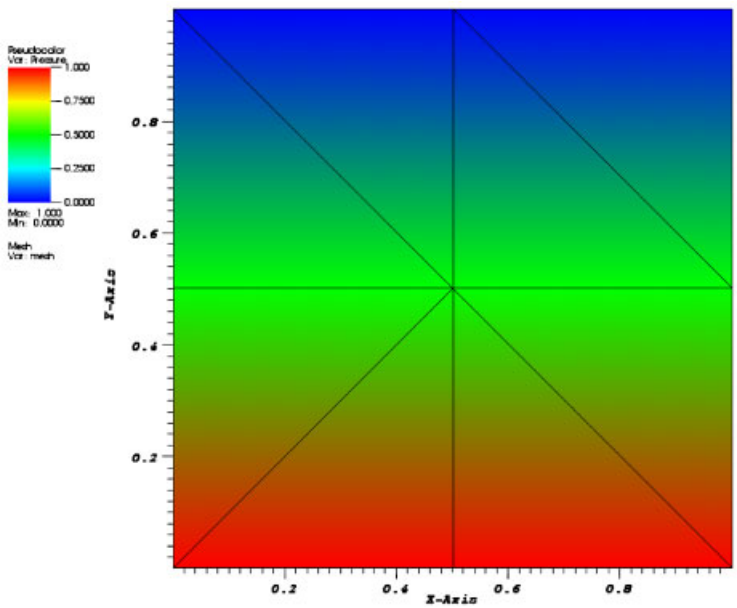

Figure 8. Square vertically split domain made of two different materials: triangular mesh used to discretize the domain and the contours for the scalar variable P.

$t = 28$ days. Figures 12 and 13 show the saturation contours for instants $t = 28$ and 48 days. The time step was fixed, with $\Delta t = 0.2$ days.

Figure 11 clearly shows the steep behaviour of the pressure field following the sudden variation of permeability that exists between the barriers and the rest of the reservoir. As expected, Figures 12 and 13 show that the fluid flow occurs essentially though the channel formed by the perpendicular barriers.

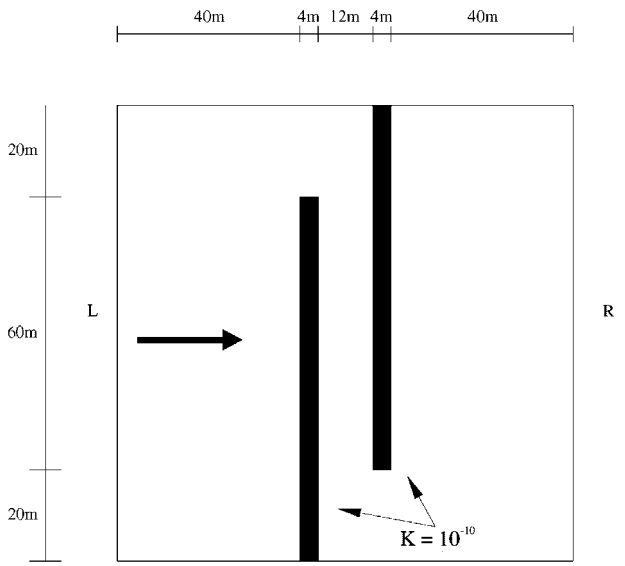

Figure 9. Geometric configuration for the problem of the confined flow between two perpendiculars barriers.

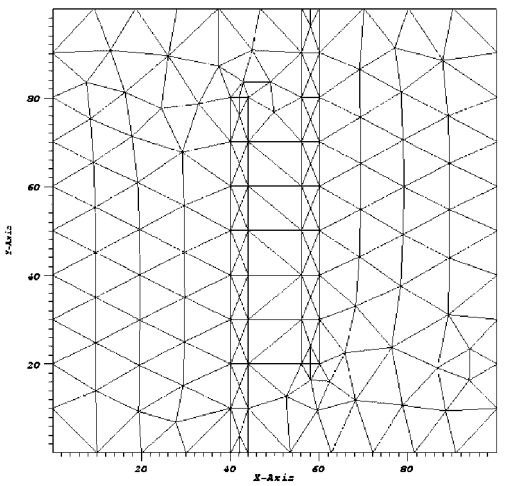

Figure 10. Confined flow between two perpendiculars barriers: triangular mesh with 156 nodes and 266 elements.

4.3. Five-spot water flood problem with a central low permeability zone

This problem, which was adapted from Helmig [30], consists in a $\frac{1}{4}$ of five-spot problem in which there is a square low permeability zone between the injection and producer wells. In this case, the low permeability zone forms a barrier that splits the fluid flow in two

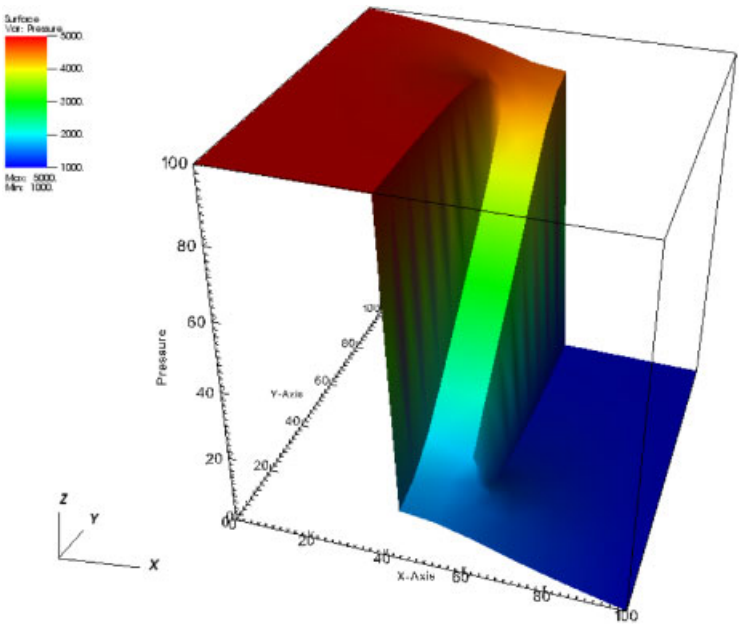

Figure 11. Confined flow between two perpendiculars barriers: pressure surface at $t = 28$ days.

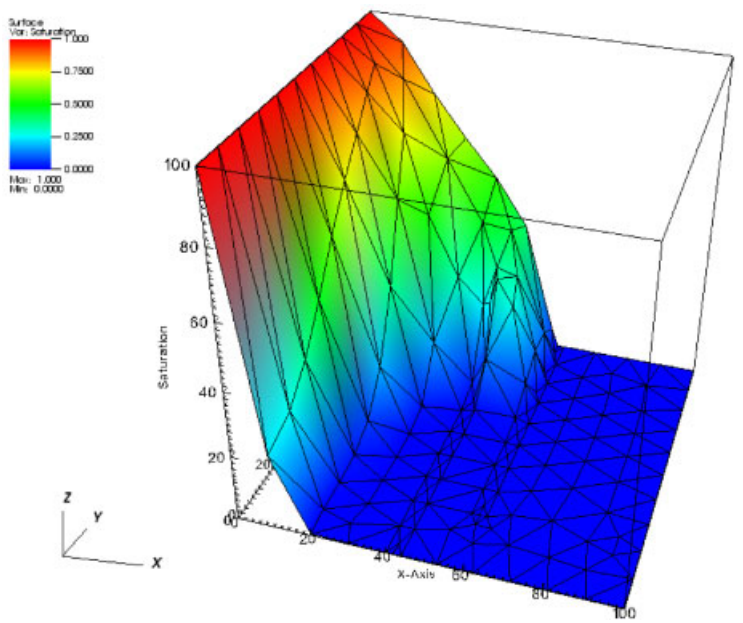

Figure 12. Confined flow between two perpendiculars barriers: saturation contours at $t = 28$ days.

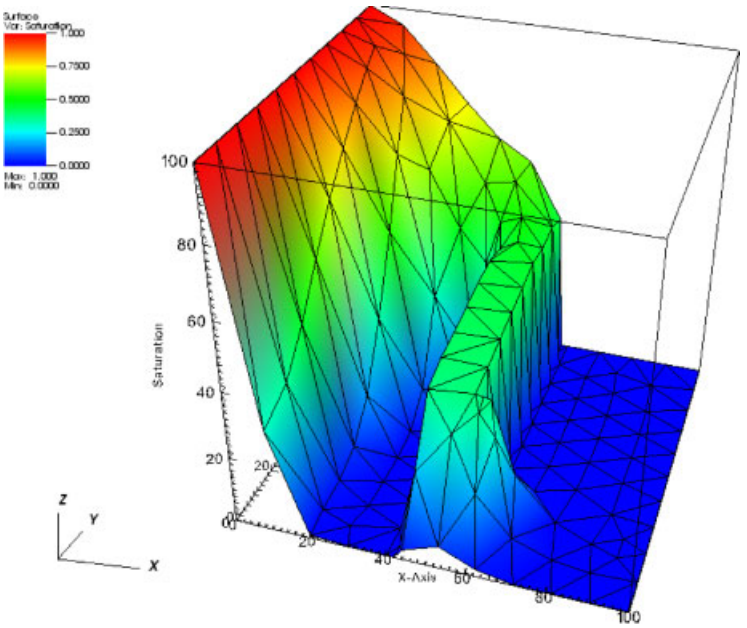

Figure 13. Confined flow between two perpendiculars barriers: saturation contours at $t = 48$ days.

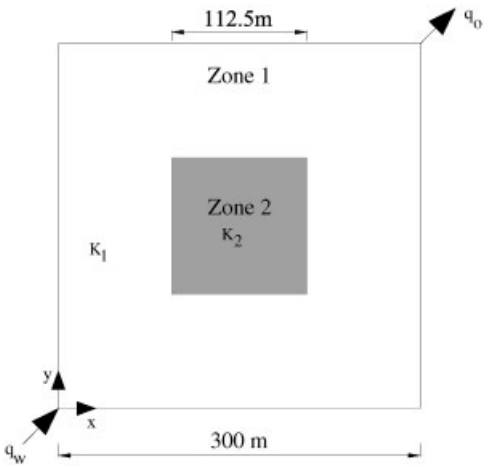

Figure 14. Geometric configuration for the problem of $\frac{1}{4}$ of five spot with a central low permeability zone.

parts. Residual saturations are $S_{rw} = S_{ro} = 0.0$ and fluid properties are $\rho_w = \rho_o = 1000\ \mathrm{kg/m^3}$ and $\mu_w = \mu_o = 0.001\ \mathrm{kg/m\,s}$. Permeability ratio is equal to 1000 with $\underset{\sim}{K}_1 = 10^{-10}\underset{\sim}{I}\ \mathrm{m^2}$ in zone 1, and $\underset{\sim}{K}_2 = 10^{-7}\underset{\sim}{I}\ \mathrm{m^2}$ in zone 2. Porosity is constant with $\phi = 0.2$ for both zones. Figure 14

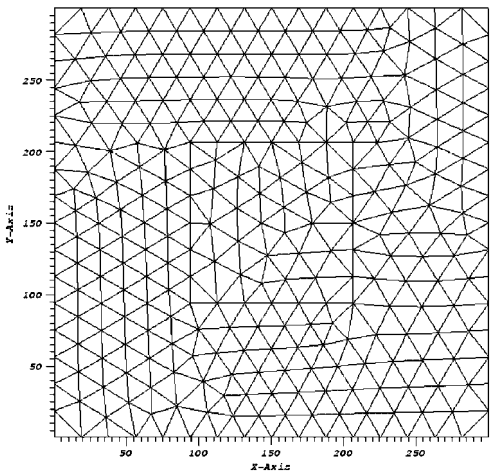

Figure 15. $\frac{1}{4}$ of five spot with a central low permeability zone: coarse mesh with 308 nodes and 550 elements.

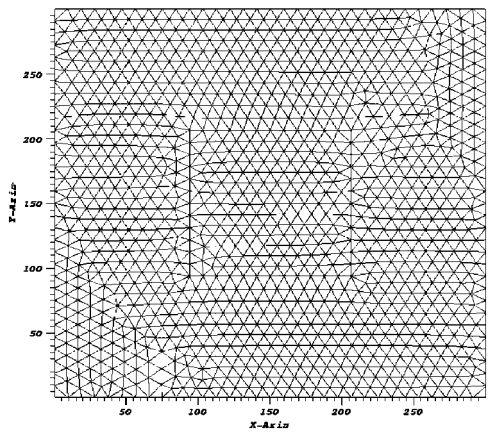

Figure 16. $\frac{1}{4}$ of five spot with a central low permeability zone: fine mesh with 1180 nodes and 2230 elements.

shows the geometric configuration of the problem. Pressure and saturation boundary conditions are, $p = 2.10^5$ Pa and $S_w = 1$ at the injection well and $Q = -10.368\,\mathrm{m}^3/\mathrm{d}$ at the producer.

For this problem we have used two different meshes. Figures 15 and 16 show, respectively, the coarse mesh, in which the mesh spacing is approximately $h \cong 18.75$ m, with 308 nodes, 550 elements and 857 edges, and the fine mesh for which $h \cong 9.375$ m, with 1180 nodes, 2230 elements and 3409 edges. Figures 17 and 18, which are in very good agreement with those of Helmig [30], show the saturation profile for both meshes at $t = 400$ days. As it can be seen, the coarse mesh is able to correctly capture the saturation front, even though results are a little bit more diffusive than in the fine mesh.

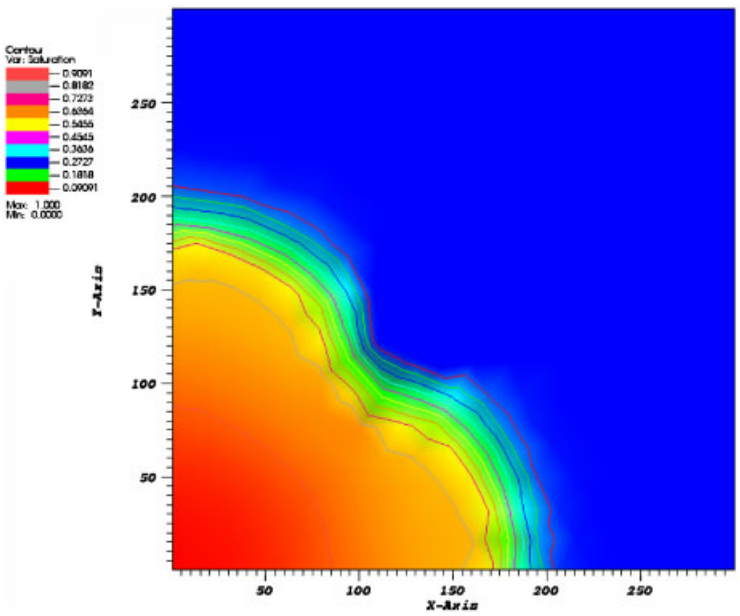

Figure 17. $\frac{1}{4}$ of five spot with a central low permeability zone: saturation contours for the coarse mesh at $t = 400$ days.

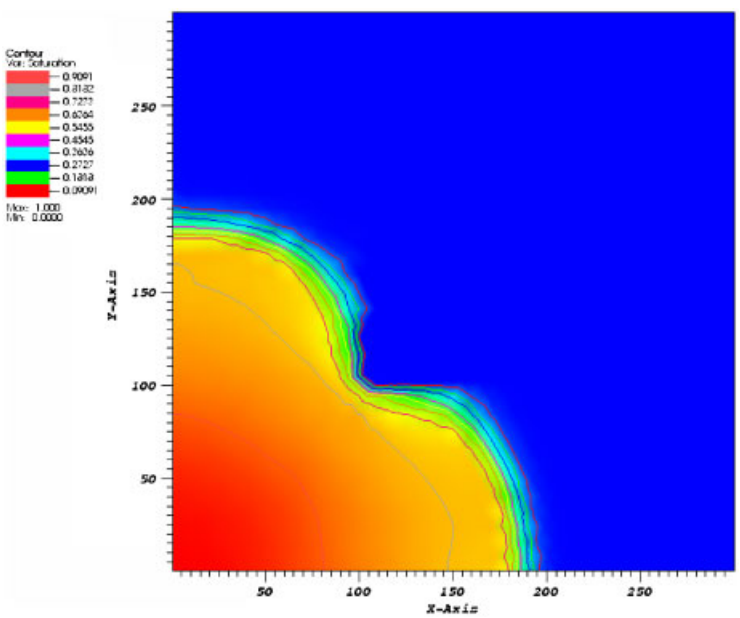

Figure 18. $\frac{1}{4}$ of five spot with a central low permeability zone: saturation contours for the fine mesh at $t = 400$ days.

5. CONCLUDING REMARKS

In this article, we have described an unstructured edge-based finite volume formulation for the solution of immiscible displacement of oil by water within non-homogeneous porous media. This FV formulation is capable of handling highly discontinuous coefficients in an elegant and accurate manner. Some representative model examples were used in order to show the ability of the proposed method to deal with discontinuous permeability fields that vary orders of magnitude throughout the reservoir formation. The artificial diffusion method used here for the solution of the saturation equation is capable of capturing water saturation fronts very accurately even for coarse meshes. Currently, we are investigating the ability of the proposed formulation to properly handle anisotropic permeability fields (full tensors) and problems with high mobility ratios. In the near future, we intend to extend this methodology to deal with more realistic problems including gravity and capillary effects in two- and three-dimensional domains.

ACKNOWLEDGEMENTS

The authors would like to thank the National Petroleum Agency (ANP) and the Brazilian Research Council (CNPq) for their financial support during the development of this work.

REFERENCES

1. Ewing RE. *The Mathematics of Reservoir Simulation*. SIAM: Philadelphia, 1983.
2. Peaceman DW. *Fundamentals of Reservoir Simulation*. Elsevier Scientific Publishing Company: Amsterdam, 1977.
3. Chen Z, Huan G, Li B. An improved IMPES method for two-phase flow in porous media. *Transport in Porous Media* 2004; **54**:361–376.
4. Chavent G, Jaffre J. *Mathematical Models and Finite Elements for Reservoir Simulation*: *Single Phase*, *Multiphase and Multicomponent Flows Through Porous Media*. Amsterdam: North-Holland, 1986.
5. Edwards MG, Rogers CF. Finite volume discretization with imposed flux continuity for the general tensor pressure equation. *Computational Geosciences* 1998; **2**:259–290.
6. Edwards MG. Unstructured control-volume distributed, full tensor finite-volume schemes with flow based grids. *Computational Geosciences* 2002; **6**:433–452.
7. Verma S. Flexible grids for reservoir simulation. *Ph.D. Thesis*, Department of Petroleum Engineering, University of Stanford/Stanford, US, 1996.
8. Verma S, Aziz K. Two and three dimensional flexible grids for reservoir simulation. *5th European Conference on the Mathematics of Oil Recovery* (*ECMOR V*), Leoben, Austria, 1996; 1–14.
9. Baoyan L, Chen Z, Guaren H. Control volume function approximation methods and their applications to modeling porous media flow. *Advances in Water Resources* 2003; **26**:435–444.
10. Loula AFD, Garcia ELM, Coutinho ALGA. Miscible displacement simulation by finite element methods in distributed memory machines. *Computer Methods in Applied Mechanics* 1999; **174**:339–354.
11. Helmig R, Huber R. Comparison of Galerkin-type discretization techniques for two-phase flow problems in heterogeneous porous media. *Advances in Water Resources* 1998; **21**:697–711.
12. Geiger S, Roberts S, Matthai SK, Zoppou C, Burri A. Combining finite element and finite volume methods for efficient multiphase flow simulations in highly heterogeneous and structurally complex geologic media. *Geofluids* 2004; **4**:284–299.
13. Durlofsky LJ. A triangle based mixed finite element—finite volume technique for modeling two phase flow through porous media. *Journal of Computational Physics* 1993; **105**:252–266.
14. Rees I, Masters I, Malan AG, Lewis RW. An edge-based finite volume scheme for saturated-unsaturated groundwater flow. *Computer Methods in Applied Mechanics* 2004; **193**:4741–4759.
15. Luo H, Baum JD, Löhner R. An improved finite volume scheme for compressible flows on unstructured grids. *Technical Report*, *AIAA Paper* 1995; 95-0348.
16. Carvalho DKE, Lyra PRM, Willmersdorf RB, Araújo FDS. An unstructured edge-based finite volume formulation for solving immiscible two-phase flows in porous media. *Communications in Numerical Methods in Engineering* 2005; **21**:747–756.

17. Crumpton PI, Moinier P, Giles MBTJ. An unstructured algorithm for high Reynolds number flows on highly stretched grids. In *Numerical Methods in Laminar and Turbulent Flow*, Taylor C, Cross JT (eds). Pineridge Press: Swansea, 1997; 561–572.
18. Sorensen KA. A multigrid accelerated procedure for the solution of compressible fluid flows on unstructured meshes. *Ph.D. Thesis*, C/PH/161/01, Department of Civil Engineering, University of Wales/Swansea, U.K., 2001.
19. Jameson A, Shmidt W, Turkel E. Numerical simulation of the euler equations by finite volume methods using Runge–Kutta time stepping schemes. *Technical Report*, *AIAA Paper*, 1981; 81-1259.
20. Peraire J, Peiró J, Morgan K. Finite element multigrid solution of euler flows past installed aero-engines. *Journal of Computational Mechanics* 1993; **11**:433–451.
21. Lyra PRM, Morgan K. A review and comparative study of upwind biased schemes for compressible flow computation. Part III: multidimensional extension on unstructured grids. *Archives of Computational Methods in Engineering* 2002; **9**(7):207–256.
22. Smith MI, Griffiths DV. *Programming the Finite Element Method*. Wiley: Chichester, 2001.
23. Muller D, Giles MB. Edge-based multigrid schemes for hybrid grids. *6th ICFD Conference on Numerical Methods for Fluid Dynamics*, Oxford, U.K., 1998; 1–7.
24. Prevost M. The streamline method for unstructured grids. University of Stanford, Department of Petroleum Engineering, *Technical Report*, 1-49, 2000.
25. Lyra PRM, Lima RCFD, Guimarães CSC, Carvalho DKE. An edge-based unstructured finite volume procedure for the numerical analysis of heat conduction applications. *Journal of the Brazilian Society of Mechanical Engineering*, *Brazil* 2004; **26**:160–169.
26. Svärd M, Nordström J. A stable and accurate summation by parts finite volume formulation of the laplacian operator. Uppsala Universitet, Institutionen für Informationsteknologi, *Technical Report 003*, 1-36, 2003.
27. Lewis RW, Malan AG. Continuum thermodynamic modeling of drying capillary particulate materials via an edge-based algorithm. *Computer Methods in Applied Mechanics* 2005; **194**:2043–2057.
28. Rees I. Development of an edge-based finite volume solver for porous media applications. *Ph.D. Thesis*, Department of Civil Engineering, University of Wales/Swansea, U.K., 2004.
29. Garcia ELM. Two and three dimensional finite element formulations for the parallel simulation of flows in petroleum reservoirs. *Ph.D. Thesis*, Department of Civil Engineering, Federal University of Rio de Janeiro, Rio de Janeiro, Brazil (in portuguese), 1997.
30. Helmig R. *Multiphase Flow and Transport Processes in the Subsurface*. Springer: Berlin, 1997.

